Journal of Pharmaceutical and Biomedical Analysis 245 (2024) 116187

Contents lists available at ScienceDirect

Journal of Pharmaceutical and Biomedical Analysis

journal homepage: www.journals.elsevier.com/journal-of-pharmaceutical-and-biomedical-analysis

Metabolism and cytotoxicity studies of the two hallucinogens 1cP-LSD and 4-AcO-DET in human liver and zebrafish larvae models using LC-HRMS/MS and a high-content screening assay

Tanja M. Gampfer [a,*], Victoria Schütz [a], Philip Schippers [a,b], Sari Rasheed [b,c], Jonas Baumann [b], Lea Wagmann [a], Benedikt Pulver [d,e,f], Folker Westphal [d], Veit Flockerzi [g], Rolf Müller [b,c], Markus R. Meyer [a]

[a] Department of Experimental and Clinical Toxicology, Institute of Experimental and Clinical Pharmacology and Toxicology, Center for Molecular Signaling (PZMS), Saarland University, Homburg, Germany
[b] Helmholtz Institute for Pharmaceutical Research Saarland (HIPS), Helmholtz Centre for Infection Research (HZI), Saarland University, Saarbrücken, Germany
[c] German Centre for Infection Research (DZIF), Partner Site Hannover, Braunschweig, Germany
[d] State Bureau of Criminal Investigation Schleswig-Holstein, Forensic Science Institute, Kiel, Germany
[e] Institute of Forensic Medicine, Forensic Toxicology, Medical Center-University of Freiburg, Faculty of Medicine, University of Freiburg, Freiburg, Germany
[f] Herrmann Staudinger Graduate School, University of Freiburg, Freiburg, Germany
[g] Department of Experimental and Clinical Pharmacology, Institute of Experimental and Clinical Pharmacology and Toxicology, Center for Molecular Signaling (PZMS), Saarland University, Homburg, Germany

ARTICLE INFO

Keywords:
New psychoactive substances
Pooled human liver S9 fraction
Zebrafish larvae
LC-HRMS/MS
HepG2
Cytotoxicity

ABSTRACT

The continuous emergence of new psychoactive substances (NPS) attracted a great deal of attention within recent years. Lately, the two hallucinogenic NPS 1cP-LSD and 4-AcO-DET have appeared on the global market. Knowledge about their metabolism to identify potential metabolic targets for analysis and their cytotoxic properties is lacking. The aim of this work was thus to study their *in vitro* and *in vivo* metabolism in pooled human liver S9 fraction (pHLS9) and in zebrafish larvae (ZL) by means of liquid chromatography-high-resolution tandem mass spectrometry. Monooxygenases involved in the initial metabolic steps were elucidated using recombinant human isozymes. Investigations on their cytotoxicity were performed on the human hepatoma cell line HepG2 using a multiparametric, fluorescence-based high-content screening assay. This included measurement of CYP-enzyme mediated effects by means of the unspecific CYP inhibitor 1-aminbenzotriazole (ABT). Several phase I metabolites of both compounds and two phase II metabolites of 4-AcO-DET were produced *in vitro* and *in vivo*. After microinjection of 1cP-LSD into the caudal vein of ZL, three out of seven metabolites formed in pHLS9 were also detected in ZL. Twelve 4-AcO-DET metabolites were identified in ZL after exposure via immersion bath and five of them were found in pHLS9 incubations. Notably, unique metabolites of 4-AcO-DET were only produced by ZL, whereas 1cP-LSD specific metabolites were found both in ZL and in pHLS9. No toxic effects were observed for 1cP-LSD and 4-AcO-DET in HepG2 cells, however, two parameters were altered in incubations containing 4-AcO-DET together with ABT compared with incubations without ABT but in concentrations far above expected in vivo concentration. Further investigations should be done with other hepatic cell lines expressing higher levels of CYP enzymes.

1. Introduction

The emergence of new psychoactive substances (NPS) is still ongoing on the global drugs of abuse market. The diverse nature of these compounds adds challenges not only to clinical and forensic toxicologists and public health agents but also to consumers by unknown health hazard. Over the last decade, NPS has earned a great deal of attention since several reports of acute poisoning and deaths have been issued [1].

* Corresponding author at: Department of Experimental and Clinical Toxicology, Center for Molecular Signaling (PZMS), Saarland University, Homburg 66421, Germany.
E-mail address: tanja.gampfer@uks.eu (T.M. Gampfer).

https://doi.org/10.1016/j.jpba.2024.116187
Received 15 November 2023; Received in revised form 18 April 2024; Accepted 26 April 2024
Available online 27 April 2024

For instance, at the end of 2022, 930 NPS were monitored by the European Monitoring Centre for Drugs and Drug Addiction of which 41 were reported for the first time [2]. Depending on the main pharmacological effects, NPS are divided into different groups including hallucinogens, stimulants, opioids, dissociatives. Two NPS belonging to the group of hallucinogens are the lysergic acid diethylamide (LSD) derivative 1-cyclopropionyl LSD (1cP-LSD) and the tryptamine-related compound 4-acetoxy-*N*,*N*-diethyltryptamin (4-AcO-DET). The difference between 1cP-LSD and LSD is an additional substitution at the N^1 position by 1-cyclopropionyl (see Fig. 1). 1cP-LSD appears to act as agonist on the 5-HT_{2A} receptor, the primary target for psychedelic effects, based on a head-twitch response (HTR) study in mice but nothing is known about the receptor pharmacology [3]. The second compound (see Fig. 2), 4-AcO-DET, showed a higher efficacy at the *in vitro* 5-HT_{2A} receptor than the naturally occurring hallucinogen *N*,*N*-dimethyltryptamine [4]. Even though 1cP-LSD has been previously identified in plotter and pellets available from online retailers and 4-AcO-DET in seized powder [3,5], an intake of both psychedelic NPS has not yet been confirmed, which may be due to lacking knowledge about suitable urinary screening targets. Unique metabolic biomarkers are required for a reliable analytical identification by e.g., liquid chromatography-high-resolution tandem mass spectrometry (LC-HRMS/MS) in human biosamples. As 1cP-LSD is known to be hydrolyzed by esterases in human serum to LSD [3], hydrolysis of 4-AcO-DET to 4-OH-DET is also expected. Although many *in vivo* NPS metabolism studies published involve rodent models [6], over the years a growing number of studies make use of one non-mammalian *in vivo* model, the zebrafish organism [7–9]. The zebrafish (*Danio rerio*) larvae (ZL) model has attracted particular interest due to special advantages such as a short reproduction time, the suitability to perform large-scale *in vivo* screenings, and their high degree of genetic conservation with humans [10–12]. Thus, drug metabolism is expected to be similar to mammals. However, establishing and maintaining a zebrafish culture facility is more costly and requires more know-how than the housing of mammals.

Besides the lack of known analytical targets for screening methods covering 1cP-LSD and 4-AcO-DET, limited data are also available concerning their (cyto-)toxic behavior, which is essential for a comprehensive risk assessment. In many cases, reports after NPS intake about acute organ damages serve as starting point for further investigations in this field. In line with the 3Rs principle (replacement, reduction, and refinement), cell-based assays are preferred to mammalian assays for toxicity testing [13]. Various cellular parameters are suitable cytotoxic indicators such as decreasing ATP content based on increasing oxidative stress levels, changes in mitochondrial membrane potential, rising cytosplasmic calcium levels, or release of intracellular components into the surrounding medium. Basically, two different test strategies exist. Conventional assays, such as the ATP bioluminescent or MTT reduction assay, measure single parameters in non-automated and separate experiments [14,15], whereas high-content screening assay (HCSA) approaches permit the simultaneous and automated analysis of multiple parameters during in a single run [16,17]. Along with their resource-efficient and time-saving qualities, automated multiplex assays have been shown to be effective in predicting human cytotoxicity [16].

The aims of the present study were the tentative identification of the phase I and II metabolites of 1cP-LSD and 4-AcO-DET by means of LC-HRMS/MS after *in vitro* pHLS9 and *in vivo* ZL incubation, the determination of the isoenzymes involved in the initial metabolic steps, and the evaluation of their cytotoxicity on HepG2 cells including metabolism-based effects using a HCSA approach.

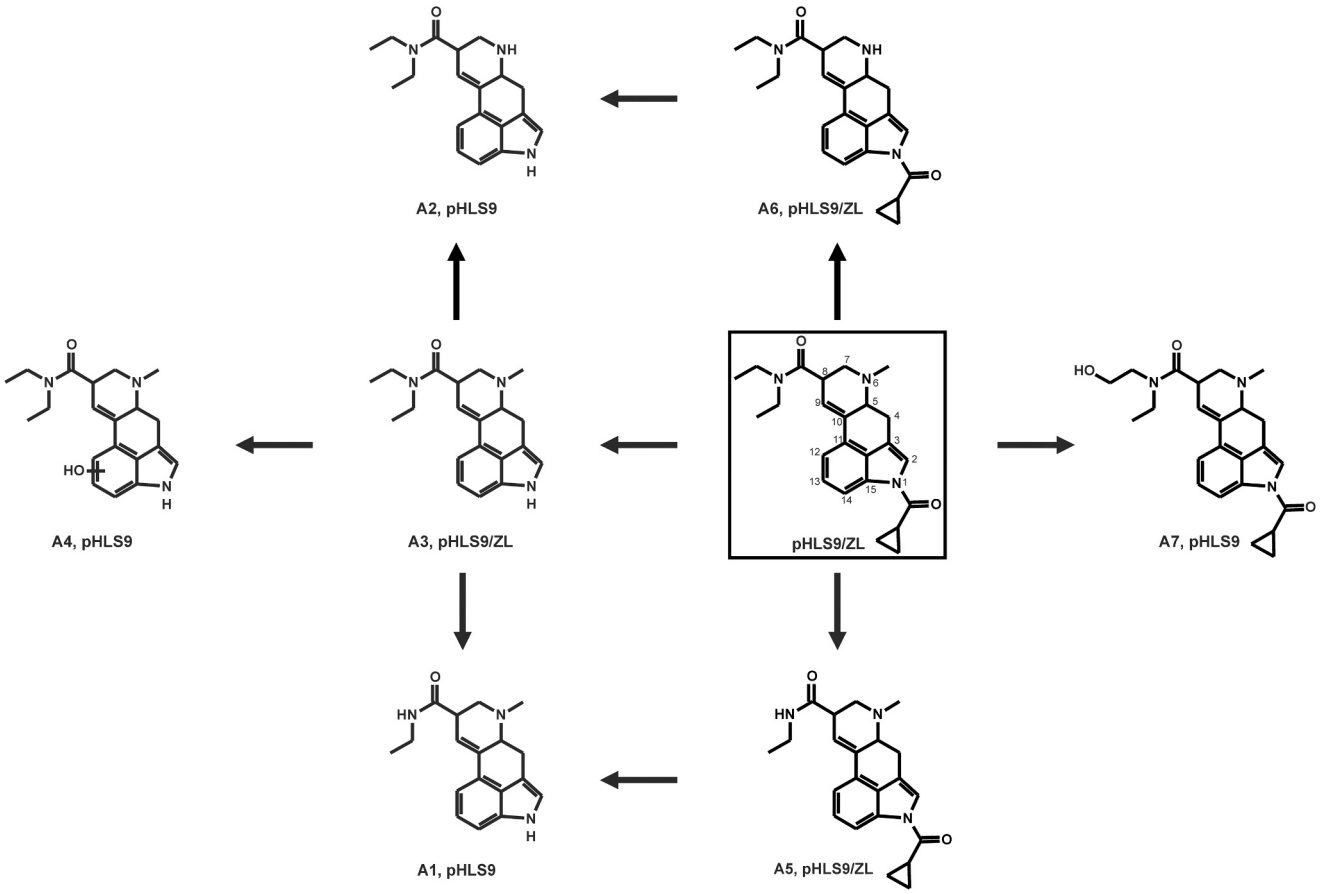

Fig. 1. Proposed *in vitro* and *in vivo* metabolic pathways of 1cP-LSD studied in pooled human liver S9 fraction (pHLS9) and zebrafish larvae (ZL) after microinjection.

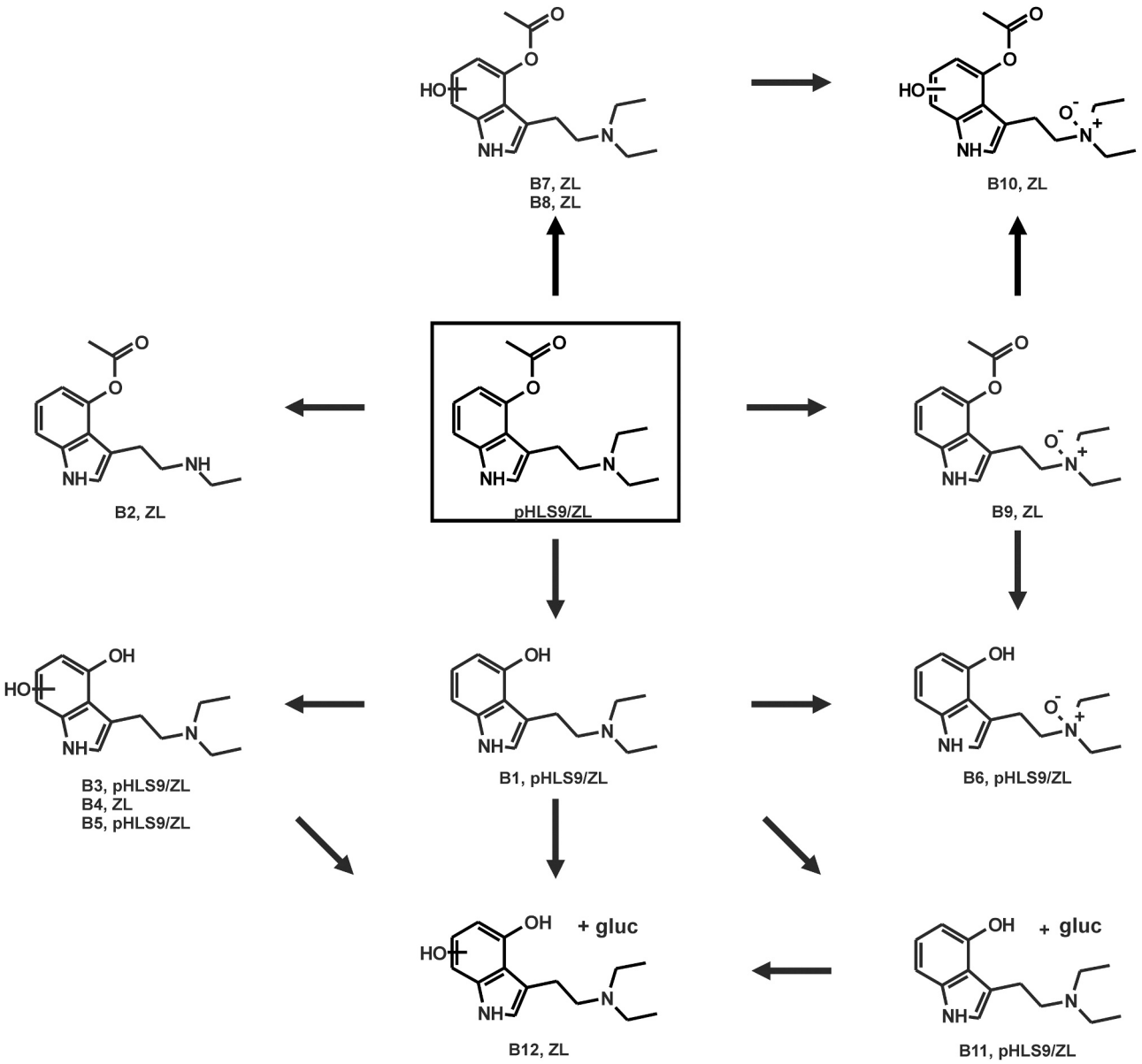

Fig. 2. Proposed *in vitro* and *in vivo* metabolic pathways of 4-AcO-DET studied in pooled human liver S9 fraction (pHLS9) and zebrafish larvae (ZL) after exposure via immersion bath.

2. Materials and methods

2.1. Chemicals and reagents

4-AcO-DET was provided as fumarate salt by the EU-funded project ADEBAR plus (Kiel, Germany, grant number IZ25–5793–2019–33) for research purposes. 1cP-LSD was purchased as free base from Toronto Research Chemicals (North York, Canada). Both NPS had a purity of at least 98 %. Hoechst33342, ionomycin, RPMI 1640 medium supplemented with GlutaMAX, sterile filters suitable for dimethyl sulfoxide (DMSO), and Tetramethylrhodamine methyl ester (TMRM) were from Life Invitrogen (Darmstadt, Germany). TOTO-3 was obtained from Fisher Scientific (Schwerte, Germany). Acetylcarnitine, acetylcarnitine transferase, acetyl coenzyme A (AcCoA), 1-aminobenzotriazole (ABT), bupropion hydrochloride, diclofenac, dipotassium hydrogen phosphate (K_2HPO_4), DMSO, ethylenediaminetetraacetic acid (EDTA), FCCP, methylene blue, penicillin, phenol red, poly-L-lysine (PLL), potassium dihydrogen phosphate (KH_2PO_4), streptomycin, tricaine, tris hydrochloride, Triton X-100, and trypsin were supplied by Sigma-Aldrich (Taufkirchen, Germany). S-(5′-Adenosyl)-l-methionine (SAM), dithiothreitol (DTT), isocitrate, isocitrate dehydrogenase, magnesium chloride ($MgCl_2$), omeprazole, 3′-phosphoadenosine-5′-phosphosulfate (PAPS), reduced glutathione (GSH), superoxide dismutase, trimipramine-d_3 (internal standard, IS), were from Merck (Taufkirchen, Germany). Dextromethorphan and phenacetin were from Roche (Grenzach, Germany) and testosterone from Fluka (Neu-Ulm, Germany). Calcium chloride ($CaCl_2$) and 4-(2-hydroxyethyl)-1-piperazineethanesulfonic acid (HEPES) were obtained by AppliChem (Darmstadt, Germany). Sodium chloride (NaCl), magnesium sulfate ($MgSO_4$), and calcium nitrate $Ca(NO_3)_2$ were purchased from Carl Roth (Karlsuhe, Germany). Potassium chloride (KCl) was bought from Grüssing (Filsum, Germany). The 75 cm^2 culture flasks and 96-well plates were from Sarstedt (Nümbrecht, Germany). CAL-520 AM and $NADP^+$ were obtained from Biomol (Hamburg, Germany). The 96-well half area high content imaging plates, acetonitrile (LC-MS grade), methanol (LC-MS grade), ammonium formate (analytical grade), formic acid (LC-MS grade), and all other reagents and chemicals (analytical grade) were from VWR International (Darmstadt, Germany). The baculovirus-infected insect cell microsomes

(Supersomes) containing 1 nmol/mL expressed human cDNA-expressed CYP1A2, CYP2A6, CYP2B6, CYP2C8, CYP2C19, CYP2D6, CYP3A4, and CYP3A5, 2 nmol/mL CYP2C9, and CYP2E1, 5 mg protein/mL flavin-containing monooxygenase 3 (FMO3), pooled human liver microsomes (pHLM, 20 mg microsomal protein/mL, 330 pmol total CYP/mg protein, 35 donors), pHLS9 (20 mg microsomal protein/mL, 30 individual donors), uridine 5′-diphospho-glucuronosyltransferase (UGT) reaction mixture solution A (25 mM UDP-glucuronic acid) and UGT reaction mixture solution B (250 mM Tris HCl, 40 mM $MgCl_2$, and 125 µg alamethicin/mL), as well as fetal bovine serum (FBS) were supplied by Corning (Amsterdam, The Netherlands). Enzymes were thawed at 37°C, aliquoted, snap-frozen in liquid nitrogen, and stored at −80 °C until use. Danieaus medium consisted of 17.4 mM NaCl, 0.21 mM KCl, 0.12 mM $MgSO_4$, 0.18 mM $Ca(NO_3)_2$, 1.5 mM HEPES and 1.2 µM methylene blue (pH 7.1–7.3). Adult zebrafish were obtained from the European Zebrafish Resource Center at Karlsruhe Institute of Technology (Karlsruhe, Germany).

HepG2 cells were purchased from the German Collection of Microorganism and Cell Cultures (DSMZ, Braunschweig, Germany). After delivery, the cells were cryopreserved and stored in liquid nitrogen at −196 °C.

2.2. pHLS9 incubations to identify in vitro phase I and II metabolites

According to a published procedure [18] with few adjustments, pHLS9 (2 mg microsomal protein/mL) was preincubated for 10 min at 37 °C with 25 µg/mL alamethicin (UGT reaction mixture solution B), 2.5 mM $MgCl_2$, 2.5 mM isocitrate, 0.8 U/mL isocitrate dehydrogenase, 0.6 mM $NADP^+$, 0.1 mM AcCoA, 2.3 mM acetylcarnitine, 8 U/mL acetylcarnitine transferase, 100 U/mL superoxide dismutase, and 90 mM phosphate buffer (pH 7.4). Afterwards, 2.5 mM UDP-glucuronic acid (UGT reaction mixture solution A), 40 µM PAPS, 1.2 mM SAM, 10 mM GSH, and 1 mM DTT were added. Reactions were started by addition of 25 µM of each NPS. Mixtures (final volume 150 µL; $n = 2$ each) were incubated for a maximum of 360 min. After 60 min a 60 µL-sample was transferred to a new reaction tube containing 20 µL ice-cold acetonitrile + 2.5 µM trimipraminde-d3 as IS to stop the reaction. The remaining mixtures were incubated for additional 300 min and thereafter stopped with 30 µL ice-cold acetonitrile + 2.5 µM trimipraminde-d3. All samples were cooled for 30 min at −20 °C and centrifuged at 18,407 x *g* for 2 min. Afterwards, the supernatants were transferred into autosampler vials and 10 µL injected onto a LC-HRMS/MS system. To exclude interfering and non-metabolically formed compounds, additional incubations were performed without NPS (blank) and without enzymes (negative control).

2.3. Zebrafish maintenance

Husbandry of adult zebrafish was carried out in accordance with internal guidelines based on the German Animal Welfare Act (§11 Abs. 1 TierSchG). Wild-type zebrafish from the AB strain were used for all investigations within the first 5 days post-fertilization (dpf) as these early devolvement stages are not considered as animal experiments according to the EU Directive 2010/63/EU [19]. Embryos were raised at 28 °C in fresh Danieau's medium.

2.4. Maximum tolerated concentration in zebrafish larvae by exposure via an immersion bath

The maximum tolerated concentration (MTC) test was conducted as previously published [20] with minor modifications. ZL at 4 dpf were collected and subdivided in 6-well plates (10 ZL/well in 3 mL Danieau's medium). NPS were administered to ZL by exposure via immersion bath at 28 °C for 24 h using the following concentrations: 0, 10, 25, 50, 75, and 100 µM containing 1 % DMSO (v/v), respectively. All incubations were done with 20 ZL. After the 24 h-incubation, ZL were investigated using a LEICA M205 FA stereo microscope (Leica Mikrosysteme Vertrieb GmbH, Wetzlar, Germany).

2.5. Zebrafish larvae incubation to identify in vivo phase I and II metabolites of 4-AcO-DET

The ZL metabolism study of 4-AcO-DET was performed as described by Park et al. [9] by exposure via immersion into bath, with minor modifications. Each well of a 6-well plate contained 10 ZL (4 dpf) in 3 mL Danieau's medium with 1 % DMSO with or without 100 µM 4-AcO-DET ($n = 2$). After incubation at 28°C for 24 h, larvae were collected separately. Twenty ZL (2 wells) were pooled into one reaction tube, washed twice with 1 mL Danieau's medium, and euthanized by placing the tubes into ice water for 15 min. Afterwards the wash solution was removed, ZL were snap-frozen in liquid nitrogen, and stored at –20 °C until use. Twenty ZL (one tube) were prepared by addition of 50 µL methanol containing 2.5 µM trimipramine-d_3 as IS, shaking for 2 min, and centrifugation at 18,407 × *g*, for 2 min. The supernatant was transferred to an autosampler vial and 10 µL were injected onto a LC-HRMS/MS system. Incubations without ZL were also performed to detect non-metabolically formed degradation products.

2.6. Zebrafish larvae microinjection to identify in vivo phase I and II metabolites of 1cP-LSD

The ZL metabolism study of 1cP-LSD was performed using microinjection as described by Park et al. [9] with minor modifications. Glass microneedles for microinjection were prepared by a Flaming/Brown type micropipette puller (Model P-100, Sutter Instrument, Novato, CA, USA) using the following settings: heat, 400 °C; ramp value, ± 10; pull, 80; velocity, 60; delay time, 105 ms; pressure, 10/20 bar. The injection solution contained 5 mM 1cP-LSD in 50:50 (v/v) DMSO:phenol red solution. After filling 10 µL of the injection solution into the microneedle using a microloader pipette tip, the needle was placed in a M-152 manipulator (Narishige Group, Tokyo, Japan) connected to a FemtoJet 4× Microinjector (Eppendorf, Hamburg, Germany). All microinjection needles were calibrated before use by injection of single droplets onto mineral oil on a micrometer slide. The injection volume was calculated according to the sphere volume equation ($V = \frac{4}{3}\pi r^3$) where r is the radius of the droplet [39,40]. An injection volume of 10 nL per ZL was chosen, which corresponds to a total amount of 705 ng 1cP-LSD in a pool of 36 larvae. Before injection, ZL (4 dpf) were placed in tricaine solution for anesthesia. Afterwards they were transferred to an object slide and the excess medium was removed. Microinjection was done into the caudal vein under a stereo microscope (LEICA M205 FA stereo microscope). After injection, ZL were incubated at 28 °C for 1 h. Thirty-six ZL were pooled prior to sample preparation. Samples were extracted as described above (Section 2.5.). All samples were prepared in duplicates. Altogether, the amount of dead ZL after microinjection was below 10 %.

2.7. Monooxygenases activity screening

In accordance with a previous publication [21], monooxygenase incubations were performed at 37 °C for 30 min using a NPS concentration of 25 µM and CYP1A2, CYP2A6, CYP2B6, CYP2C8, CYP2C9, CYP2C19, CYP2D6, CYP2E1, CYP3A4, CYP3A5 (50 pmol/mL each), or FMO3 (0.25 mg protein/mL). Besides incubation mixtures (final volume 50 µL; $n = 2$ each) contained 90 mM phosphate buffer (pH 7.4), 5 mM $MgCl_2$, 5 mM isocitrate, 1.2 mM $NADP^+$, 0.5 U/mL isocitrate dehydrogenase, and 200 U/mL superoxide dismutase. Incubations of CYP2A6 and CYP2C9 contained 90 mM Tris buffer instead of phosphate buffer as recommended by the manufacturer. Reactions were started by addition of monooxygenases and stopped after 30 min by addition of 50 µL of ice-cold acetonitrile containing 2.5 µM trimipramine-d_3 as IS. Afterwards the samples were centrifuged for 5 min at 18,407 x *g* the

supernatants were transferred into autosampler vials, and 10 μL were injected onto the LC-HRMS/MS system. Incubations with pHLM (2 mg microsomal protein/mL) and incubations without any enzymes were used as positive and negative controls.

2.8. LC-HRMS/MS settings

The LC-HRMS/MS system consisted of a Thermo Fisher Scientific (TF, Dreieich, Germany) Q-Exactive MS equipped with a heated electrospray ionization (HESI)-II source coupled to a TF Dionex UltiMate 3000 RS LC system comprising a degasser, a quaternary pump, and an HTC PAL autosampler (CTC Analytics AG, Zwingen, Switzerland). According to the manufacturer's recommendations, a mass calibration was done prior to analysis. A TF Accucore Phenyl-Hexyl column (100 mm × 2.1 mm, 2.6 μm) was used for gradient elution at 40 °C according to Richter et al. [22]. The mobile phases for gradient elution were composed of 2 mM aqueous ammonium formate plus formic acid (0.1 %, v/v, pH 3, eluent A) and 2 mM ammonium formate solution with acetonitrile:methanol (1:1, v/v), water (1 %, v/v), and formic acid (0.1 %, v/v, eluent B). The gradient settings were as follows: from 0 to 1 min hold 99 % A, from 1 to 10 min to 1 % A, from 10 to 11.5 min hold 1 % A, and from 11.5 to 13.5 min hold 99 % A. The flow rate was kept at 500 μL/min from 0 till 10 min and 800 μL/min from 10 till 13.5 min. The following HESI-II source settings were used: heater temperature, 320 °C; ion transfer capillary temperature, 320 °C; spray voltage, 4.0 kV; ionization mode, positive; sheath gas, 60 arbitrary units (AU); auxiliary gas, 10 AU; sweep gas, 0 AU; S-lens RF level, 60.0. The MS operated in full scan (FS) mode followed by a subsequent data-dependent acquisition of MS^2 (ddMS2) mode with priority to mass to charge ratios (m/z) of the parent compound and expected metabolites. FS data acquisition settings were as follows: resolution, 35,000 FWHM at m/z 200; microscans, 1; automatic gain control (AGC) target, 1e6; maximum injection time (maxIT), 120 ms; scan range, m/z 100–930. $ddMS^2$ mode settings were as follows: option "pick others", enabled; dynamic exclusion, feature not used; resolution, 17,500 FWHM at m/z 200; microscans, 1; isolation window, m/z 1.0; loop count, 5; AGC target, 2e5; maxIT, 250 ms; high collision dissociation cell with stepped normalized collision energy, 17.5, 35.0, 52.5; exclude isotopes, on; spectrum data type, profile. An inclusion list containing m/z values of expected phase I and II metabolites of 4-AcO-DET and 1cP-LSD, such as hydrolysis products, dealkyl- and hydroxy- metabolites, as well as sulfates and glucuronides, was used for ddMS2 mode. ChemSketch 2023.1.1 (ACD/Labs, Toronto, ON, Canada) was used to draw chemical structures of 4-AcO-DET, 1cP-lSD, and their predicted metabolites, as well as to calculate the exact masses. TF Xcalibur Qual Browser 4.1.31.9 was used for MS data analysis.

2.9. Cytotoxicity studies using HepG2 cells

2.9.1. Cell culture

According to an established procedure [23], HepG2 cells were maintained in 75 cm^2 flasks using RPMI 1640 medium with the following additives as recommended by the manufacturer: 100 U/mL penicillin, streptomycin, and 10 % FBS. Cell cultures were kept at 37 °C with 95 % air humidity and 5 % CO_2 atmosphere. Cells were handled under sterile conditions. Cells were passaged every 3−4 days using PBS solution (137 mM NaCl, 2.7 mM KCl, 1.5 mM KH_2PO_4, 8.1 mM $Na2HPO_4$, pH 7.4) and 0.05 % (v/v) trypsin EDTA solution. Passage number 14 was used for all experiments.

2.9.2. Preparation of cell plates for cytotoxicity testing

Cell plates were prepared based on a previous study [23], using black 96-well half area plates, which were coated with 100 μL aqueous PLL (100 μg/mL) and incubated for 30 min at 21°C. Thereafter, the plates were washed once with 150 μL autoclaved water and twice with 150 μL RPMI medium. Afterwards cells were counted using a hemocytometer, 100 μL cell suspension was transferred to the previously coated plate (density 1.750 $\times 10^4$ cells/well), and incubated for 24 h at 37 °C, 95 % air humidity, and 5 % CO_2 atmosphere.

2.9.3. Inhibition potential of ABT on CYP enzymes

To determine the inhibition potential of ABT on HepG2 cells a CYP substrate cocktail assay was adapted [24]. Cell plates were prepared as described in Section 2.9.2., but cells were seeded at a density of 7.0 $\times 10^4$ using standard 96-well plates. After the 24 h-incubation at 37 °C, 95 % air humidity, and 5 % CO_2 atmosphere, CYP substrates were freshly prepared in RPMI medium with additives containing ABT in different concentrations (50 – 1000 μM). The following six compounds were included: 12 μM phenacetin (CYP1A2), 30 μM bupropion (CYP2B6), 3.5 μM diclofenac (CYP2C9), 21 μM omeprazole (CYP2C19), 8.5 μM dextromethorphan (CYP2D6), and 86 μM testosterone (CYP3A). Supernatants (100 μL) of the cell media were removed and 100 μL of the CYP substrate ABT cocktail were added. All incubations were done fivefold. Negative control incubations without CYP substrate cocktail and ABT as well as without HepG2 cells were performed to exclude interfering and non-metabolically formed compounds. Additionally, blank incubations with CYP substrates but without ABT were prepared to evaluate the general CYP enzyme activity of HepG2. In total, plates were incubated for 1 h at 37°C, 95 % air humidity, and 5 % CO_2 atmosphere. Afterwards, supernatants were transferred to another 96-well plate and stored at −20°C until use. After removal of the media from each well, cells were washed with 100 μL PBS and 50 μL in-house manufactured RIPA buffer (150 mM NaCl, 50 mM Tris HCl pH 7.5 mM EDTA, 1 % Nonidet P-40, 0.1 % SDS, and 0.5 % sodium deoxycholate) was added before collecting the cell lysate. The protein amount of samples was determined in duplicate at 540 nm using a commercial kit (Pierce BCA Protein Assay, Fisher Scientific, Schwerte, Germany) according to a standard in-house protocol.

Cell media (50 μL) were precipitated with 75 μL acetonitrile containing trimipramine-d3 (2.5 μM) as IS. After centrifugation at 18,407 x g for 2 min, supernatants were transferred into autosampler vials, and 10 μL were injected onto the LC-HRMS/MS system. Measurement parameters of the LC-HRMS/MS system were the same as described in Section 2.8. using an adjusted inclusion list consisting of CYP substrates and the following monitored metabolites: *O*-deethyl phenacetin (CYP1A2), 4-hydroxy bupropion (CYP2B6), 4-hydroxy diclofenac (CYP2C9), 5-hydroxy omeprazole (CYP2C19) *O*-demethyl dextromethorphan (CYP2D6), and 6-beta-hydroxy testosterone (CYP3A).

2.9.4. Cytotoxic effects of ABT

For the cytotoxicity testing of ABT, sterile stock solutions were prepared 200-fold concentrated in DMSO. ABT dilutions (50 – 1000 μM) were freshly prepared in tubes and 96-well plates using RPMI medium with additives. Cell plates were prepared according to Section 2.9.2. Supernatants (100 μL) of the cell plates were removed and 100 μL of each ABT concentration was added. Blank incubations were also prepared without ABT but 0.5 % (v/v) DMSO. Each concentration was incubated five-fold. Plates were incubated for 48 h at 37 °C with 95 % air humidity and 5 % CO2 atmosphere. After a 48 h-incubation at 37 °C, 95 % air humidity, and 5 % CO_2 atmosphere, the supernatants were removed and 75 μL of a fluorescence dyes cocktail (0.8 μM Hoechst33342, 1 μM CAL-520, 20 nM TMRM, and 1 μM TOTO-3) in RPMI medium were added. Plates were incubated protected from light for 1 h at 37 °C, 95 % air humidity, and 5 % CO_2 atmosphere. Afterwards cells were washed three times with 50 μL ringer solution (140 mM NaCl, 2.8 mM KCl, 2 mM $MgCl_2$, 1 mM $CaCl_2$, 10 mM HEPES, pH 7.4). The last 50 μL remained on the cells throughout the analysis.

2.9.5. Cytotoxicity of hallucinogenic NPS

Cell plates were prepared according to Section 2.9.2. The general procedure was based on a previous study [23], with minor modifications, Final test concentrations of 4-AcO-DET were 7.81 and 125 μM

whereas 1cP-LSD was tested in 3.15 and 50 μM concentrations due to its insolubility in higher concentrations. Test solutions containing additional 500 μM ABT with NPS were also prepared. All incubations were done fivefold. Additionally, all wells contained 0.5 % (v/v) DMSO. Supernatants (100 μL) of the cell plates were removed and 100 μL of the NPS solution was added. Incubations without NPS and without NPS but ABT were prepared as negative controls and FCCP, ionomycin, and Triton-X 100 as positive controls, respectively. Drug plates were incubated for 48 h at 37 °C with 95 % air humidity and 5 % CO_2 atmosphere. Treatment with the fluorescence dyes cocktail and the subsequent washing step were the same as described in Section 2.9.4.

2.9.6. Microscope parameters

A BioTek (BT) Lionheart FX Automated Microscope (Agilent Technologies, Santa Clara, CA; USA) was used for cell plate analysis equipped with an environmental control cover as described earlier [23]. The environmental conditions were kept constant at 37 °C with a temperature gradient (2 °C) without extra CO_2 during image acquisition. To prevent evaporation, microplate lids were left on the cell plates. A 20x/0.45 (semi-apochromat) objective was used for image recording. Excitation and emission wavelengths of fluorescence dyes were as follows: 377 and 447 nm (Hoechst33342), 469 and 525 nm (CAL-520), 531 and 593 nm (TMRM), and 628 and 685 nm (TOTO-3). First Hoechst33342 was recorded in the first channel by the autofocus mode followed by CAL-520, TMRM, and TOTO-3. The following camera settings were used: LED value, 1 (Hoechst33342 and CAL-520) and 2 (TMRM and TOTO-3); camera gain, 24 dB; integration time (IT), Hoechst3342, 240 ms; TMRM, 1000 ms; CAL-520, 200−564 ms; TOTO-3, 1000−1500 ms. Before measuring the whole cell plate, the IT was checked using single blank wells, and if necessary adapted. Six images per well were recorded in a fixed distance in between. Each compound was measured within 60 min.

2.9.7. Data capture and image analysis

Data capture and image analysis was consistent with a published procedure [23], using the Agilent BT Gen5 Image Prime 3.14 software. The following data were collected: cell count, nuclear size, and nuclear intensity were determined by the area and fluorescence intensity of Hoechst33342; intracellular calcium levels was measured by the intensity of CAL-520; mitochondrial membrane potential was defined by intensity of TMRM; and TOTO-3 fluorescence intensity was measured to assess the plasma membrane permeability. Pre-processing filters and intensity thresholds were applied to define nuclei as individual units or regions of interest. Thereafter, a manual image inspection was conducted by the nuclei fluorescence Hoechst33342 to identify and exclude images containing blurriness or artifacts. The total fluorescence intensities of Hoechst3342, CAL-520, TMRM, and TOTO-3 were normalized automatically to the cell count. After the data were transferred to Microsoft Excel 2016 (Microsoft Corporation, WA, USA), the number of objects was normalized manually to the number of used images per well.

2.9.8. Statistical analysis

GraphPad Prism 5.00 (GraphPad Software, San Diego, CA, USA) was used for statistical analysis. Data are presented as mean ± standard error of the mean (SEM). One-way ANOVA followed by Tuckeýs post hoc test was used with a significance level of 0.05 (95 % confidence interval) to compare blank incubations with all other incubations and same concentrated NPS incubations without ABT to the same concentrated NPS incubations with ABT.

3. Results and discussion

3.1. Identification of in vitro phase I and II metabolites in pHLS9 incubations

Identification of metabolic biomarkers was first done by screening for potential exact precursor ions (PI) in the FS data of expected metabolites. Afterwards, the fragmentation pattern of the MS^2 spectra were analyzed and compared with that of the respective parent compound for confirmation. Since reference material for the postulated metabolites of 1cP-LSD and 4-AcO-DET was not available at the time of the study, the metabolic transformation could not be confirmed using chemical standards. All tentative identified *in vitro* or *in vivo* phase I and II metabolites of 1cP-LSD and 4-AcO-DET are listed in Table S1 and S2 in the Electronic Supplementary Materiel (ESM). In addition, their ID, metabolic reaction, the measured mass of PI and fragment ions (FI), elemental composition, calculated exact mass of the protonated PI and FI, mass error, and retention time (Rt) are also contained. In total, seven and twelve metabolites were detected for 1cP-LSD and 4-AcO-DET, respectively. MS^2 spectra of 1cP-LSD and 4-AcO-DET and their tentatively identified metabolites are presented in Fig. S1 and S2 in the ESM. Proposed *in vitro* and *in vivo* metabolic pathways of 1cP-LSD and 4-AcO-DET are depicted in Figs. 1 and 2.

MS^2 data of 1cP-LSD have been previously published by Brandt et al. [3] using ESI quadrupole time of flight tandem mass spectrometry. These were in accordance with the observed fragmentation pattern of 1cP-LSD obtained after orbitrap-based tandem mass spectrometry. MS^2 spectra of 1cP-LSD and its identified metabolites can be found in Fig. S1 in the ESM. In the following section exact calculated masses are used to describe fragments in MS^2 spectra of 1cP-LSD and tentative metabolites. The 1 cP-LSD spectrum (PI at *m/z* 392.2332) contained compound specific features, e.g., the first FI at *m/z* 349.1910 was formed after the loss of *N*-methylmethanimine from the ergoline core structure. A loss of the *N*,*N*-diethylformamide from the intact precursor molecule led to FI at *m/z* 291.1491 and the cleavage of the 1-cyclopropanoyl group corresponded to the FI at *m/z* 69.0334. These fragments allowed for a differentiation between 1cP-LSD and 1 P-LSD as they contain the 1-cyclopropanoyl substituent in comparison to 1-propionyl moiety for 1 P-LSD. All other fragments were consistent with those reported for 1 P-LSD [25]. The high abundant fragment FI at *m/z* 223.1229 suggested a loss of the 1-cyclopopionyl part from FI at *m/z* 291.1491. As mentioned by Brandt et al. [3], two comparable abundant FI at *m/z* 208.0756 and at *m/z* 208.0994 ($C_{14}H_{12}N_2^+$, not labeled in the spectrum in Fig. S1) were both present in the spectrum of 1cP-LSD. The formation of FI at *m/z* 208.0756 could be explained by a loss of the *N*,*N*-diethylamine group and the 1-cyclopropanoyl moiety [3]. A mass shift of 15.0234 u of the second-named FI corresponded to a loss of methyl radical from the N^6-methylated ergoline core with FI at *m/z* 223.1229. In addition, FI at *m/z* 197.1073 was in accordance with FI at *m/z* 223.1229 altered by a loss of an ethinyl group from the remaining ergoline core. Both FI at *m/z* 128.1069 and *m/z* 74.0964 representing the diethylamide part were observed in the spectrum of 1cP-LSD.

Seven phase I metabolites and no phase II metabolites of 1cP-LSD were identified in pHLS9. Negative controls and blank incubations of 1cP-LSD showed no interferences. The MS^2 spectrum of metabolite A1 (PI at *m/z* 296.1757) indicated a *N*-deacetylation at the N^1-acyl substituent coupled with *N*-deethylation at the *N*,*N*-diethylamine group. The missing fragments of the 1-cyclopropanoyl (*m/z* 69.0334) and *N*,*N*-diethylamine part (*m/z* 74.0964) together with unchanged high abundant FI at *m/z* 223.1229, *m/z* 208.0756, and *m/z* 197.1073 compared with the 1cP-LSD spectrum supported this assumption. *N*-deacetylation combined with *N*-demethylation on N^6 led to the emergence of metabolite A2 (PI at *m/z* 310.1913). Characteristic features with FI at *m/z* 237.1022 and at *m/z* 209.1073 corresponded to FI at *m/z* 253.1339 and at *m/z* 223.1229 of *N*-deacyl 1cP-LSD shifted either by loss of a methyl group. In addition, FI at *m/z* 69.0334 representing the 1-acyl substituent was not present in the spectrum of A2. Based on the formation of LSD after incubation of 1cP-LSD with human serum by Brandt et al. [3], metabolic formation of LSD was also expected in our study. LSD (A3, PI at *m/z* 324.2070) was formed after *N*-deacetylation of 1cP-LSD. The spectra of LSD and 1cP-LSD were much alike, except of FI at *m/z* 281.1648 which corresponded to FI at *m/z* 349.1910 shifted by the mass

of the 1-acyl substituent. Furthermore, the 1-cyclopropanoyl moiety (*m/z* 69.0334) did not appear in its spectrum. Hydroxylation of LSD (A3) at the ergoline core resulted in the formation of 1-deacyl-hydroxy 1cP-LSD (A4, PI at *m/z* 340.2019). Fragments consisting of the ergoline core structure were all shifted by a mass of +15.9949 u compared with LSD (A3), e.g., FI at *m/z* 239.1178 and at *m/z* 224.0706. Hydroxylation most likely proceeded at the ergoline ring system but the final position could not be determined based on the fragmentation pattern. All previously mentioned metabolites could also originate from LSD or other analogues [25]. One of the 1cP-LSD-specific metabolites was formed by *N*-deethylation (A5) with PI at *m/z* 364.2019. The MS^2 spectrum of *N*-deethylated metabolite contained two divergent fragments with FI at *m/z* 349.1784 and *m/z* 321.1597 compared with 1cP-LSD. The mass of the former one corresponded to a loss of a CH_3 at the N^6-methylated ergoline core. The latter fragment correlated with FI at *m/z* 349.1910 shifted by a mass of +28.0313 u matching with the missing vinyl group of *N*-deethyl 1cP-LSD. In addition, the lack of FI at *m/z* 74.0964 representing the diethylamide part affirmed this presumption. Unexpectedly, FI at *m/z* 100.0756, originally assigned by Brandt et al. to the *N,N*-diethylformamide moiety [3], was present in the spectrum of all metabolites including a *N*-deethylation pointing towards another structural origin. Most likely this fragment consisted of the *N*-ethylpropanamide residue corresponding to FI at *m/z* 128.1069 shifted by an ethyl group. *N*-Demethylation at N^6 of the ergoline core resulted in the formation of *N*-demethyl 1cP-LSD (PI at *m/z* 378.2176, A6). Descriptive MS^2 fragments were the high abundant FI at *m/z* 277.1335 and at *m/z* 209.1073 corresponding to FI at *m/z* 291.1491 and at *m/z* 223.1229 minus methylene (14.0156 u, CH_2). Unaltered FI at *m/z* 128.1069 consisting of the *N*-ethylpropanamide moiety and FI at *m/z* 74.0964 representing the *N,N*-diethylamine part confirmed this assumption. One hydroxy metabolite (A7) was identified with PI at *m/z* 408.2281, but surprisingly with a MS^2 spectrum divergent from that of *N*-deeacyl-hydroxy 1cP-LSD (A4). The hydroxy group was positioned at the *N,N*-diethylamine part owing to the FI at *m/z* 90.0913 and at *m/z* 72.0807 originating from the hydroxylated *N,N*-diethylamine part both before and after water loss together with the otherwise unchanged spectrum compared with 1cP-LSD. Most probably, the hydroxy group was located at one of the terminal CH_3 groups at the *N,N*-diethylamine part as hydroxylation at the carbon atom next to the amide would lead to an potentially instable carbinolamide structure [26]. All seven aforementioned phase I metabolites were identified in pHLS9 incubation both after 1 h and 6 h, except of metabolite A2 (*N*-deacyl-*N*-demethyl-) which was only found after an incubation of 6 h. *In vitro* phase II metabolism seemed to play a minor role which was in accordance with similar findings for the related LSD derivative 1 P-LSD using pHLS9 [25].

The MS^2 spectrum of 4-AcO-DET (PI at *m/z* 275.1754) contained a FI at *m/z* 202.0862, which could be assigned to the 4-AcO-ethylindol part after loss of the *N,N*-diethylamine. An additional loss of the acetaldehyde group led to FI at *m/z* 160.0756. Further cleavage of a CO group (–27.9949 u) resulted in FI at *m/z* 132.0807 indicating a rearrangement at the indole ring by size reduction to a cyclopentapyrrole as described for 5-OH-tryptamine [5]. The most abundant FI at *m/z* 86.0964 consisted of *N,N*-diethylmethylamine after C-C bond cleavage at the ethyl linker. Also FI at *m/z* 58.0651 corresponded to the *N,N*-diethylmethylamine part of the molecule with additional loss of C_2H_5.

Four phase I and one phase II metabolites of 4-AcO-DET could be detected in pHLS9 incubations. No interfering signals were observed in blank incubations. Tryptamines are prone to display instability [27], therefor it was not surprising to find multiple metabolites of 4-AcO-DET in all negative controls. A higher abundance of potential metabolites in enzyme-containing incubations than in negative controls was required for a positive identification. Single *O*-deacetylation led to 4-OH-DET with PI at *m/z* 233.1648 (B1). The only dissimilarity to the 4-AcO-DET spectrum was the missing FI at *m/z* 202.0862 corresponding to the ethylindol part with intact ester structure. Ester hydrolysis coupled to hydroxylation at the indole led to three potential *O*-deacyl-hydroxy isomers (B3, B5, B6, PI at *m/z* 249.1597). The first two isomers showed a high correlation of their MS^2 spectra with FI at *m/z* 176.0706 shifted by one oxygen (+15.9949 u) compared with FI at *m/z* 160.0756 in the parent spectrum. This fact together with a lack of a water loss suggested a hydroxylation at the indole core. An additional indicative fragment was FI *at m/z* 148.0393 in the spectrum of B3 representing the dihydroxy-indole core. The last isomer showed a divergent fragmentation pattern as the other isomers with unchanged core structure described by FI at *m/z* 160.0756, at *m/z* 132.0807, and at *m/z* 115.0542 compared with the parent spectrum. Furthermore, the lack of an initial water loss and the relatively late Rt compared with the other isomers pointed to an *O*-deacetyl-*N*-oxide. The only phase II metabolite was formed by *O*-deacetylation followed by glucuronidation (B11, PI at *m/z* 409.1969). The MS^2 spectrum contained one specific FI at *m/z* 233.1648 corresponding to the *O*-deacetyl-hydroxy molecule after loss of the glucuronide. All other fragments were consistent with the *O*-deacetyl metabolite B1. All five described metabolites were identified in the pHLS9 incubation both after 1 h and 6 h.

3.2. Maximum tolerated concentration test in zebrafish larvae

A MTC test was performed in advance to the ZL metabolism study to ensure that no ZL were intoxicated which may alter their metabolism. Treatment of ZL (4 dpf) with 100, 75, and 50 μM 1cP-LSD resulted in no viable ZL after 24 h. Even at 25 μM 1cP-LSD some ZL seemed intoxicated showing morphological anomalies such as a curved tail or changes in behavior, e.g., lethargy. Noteworthy, acute toxic effects of 1cP-LSD were rather unexpected since results from a previous MTC test of the structural related compound 1P-LSD gave no grounds for an acute toxicity of LSD analogs on ZL [18]. While it could be supposed that the substitution of the 1-propionyl residue of 1P-LSD by a 1-cyclopropanoyl group leading to 1cP-LSD might be the cause for different effects, the tested concentrations seemed far too high to be of relevance for 1cP-LSD intoxications in humans based on LSD plasma concentrations [28]. Owing to the MTC test result, the 1cP-LSD concentration must be adapted for the ZL metabolism study, however, it remained doubtful whether metabolites could be detected in concentrations below 25 μM. Hence, an alternative administration route was selected via microinjection into the caudal vein, which has been shown promising results in the total number of detected metabolites of a synthetic cannabinoid [9].

The survival rate of 4-AcO-DET treated ZL were 100 % in all tested concentrations. Therefore, the metabolism experiment was conducted by immersion of larvae into medium containing 100 μM 4-AcO-DET.

3.3. Identification of in vivo metabolites in zebrafish larvae

ZL represent an alternative model than mammals for studying the *in vivo* metabolism of NPS not only with regard to 3Rs but also as demonstrated in several studies by a good agreement with human metabolism [8,9,11,18]. Apart from holding direct orthologs for CYP enzymes [29], also cholin- and carboxylesterases activity is described at this stage of larvae development [30]. 1cP-LSD was administered to ZL via microinjection into the caudal vein due to its high toxicity by aquatic exposure. Only three phase I metabolites already described in Section 3.1. could be detected in ZL after microinjection followed by 1 h-incubation, namely *N*-deacyl (A3), *N*-deethyl (A6), and *N*-demethyl 1cP-LSD (A7). Most probably this low number of identified metabolites was due to too a short incubation time after microinjection.

In total, 10 phase I and two phase II metabolites of 4-AcO-DET were identified i*n vivo* including all above mentioned metabolites (Section 3.1.). The first newly detected metabolite was formed by *N*-deethylation (PI at *m/z* 247.1441, B2). The MS^2 spectrum was comparable with the parent spectrum with the difference in additional low abundant FI at *m/z* 190.0862 and at *m/z* 148.0756. The first-mentioned fragment was formed by loss of C_3H_7N from the *N,N*-diethylamine residue and the second by an additional loss of the acetyl group. Another *O*-deacetyl-

hydroxy isomer (B4) was formed by ZL (PI at *m/z* 249.1597, B4) showing similar fragmentation than the other isomers (B3, B5). The mere presence of FI at *m/z* 120.0443 corresponding to the rearranged hydroxy-bicyclic ring system after CO loss, led to the conclusion that the hydroxylation proceeded at the indole core. Metabolites B7, B8, and B9 were detected with PI at *m/z* 291.1703 corresponding to a single hydroxylation of 4-AcO-DET. MS^2 spectra of B7 and B8 showed a high degree of matching fragments, e.g., FI at *m/z* 218.0811 correlated with FI at *m/z* 202.0862 and FI at *m/z* 176.0706 with FI at *m/z* 160.0756 in the parent spectrum both shifted by one oxygen (+15.9949 u). Together with unchanged small fragments carrying the *N,N*-diethylamine part and no observed water loss, this indicated a hydroxylation at the indole core. The fragmentation pattern of B9 correlated to them of the *O*-deacetyl-*N*-oxide B6 with the difference in FI at *m/z* 202.0862 representing the remaining molecule after *N,N*-diethylamine hydroxy cleavage which was not present in the spectrum of the aforementioned *O*-deacetyl-*N*-oxide metabolite. *N*-Oxidation plus additional hydroxylation was the supposed metabolic reaction leading to metabolite B10 (PI at *m/z* 307.1652). Characteristic FI at *m/z* 218.0811 and at *m/z* 176.0706 corresponded to FI at *m/z* 202.0862 and at *m/z* 160.0756 of the *N*-oxide (B9) shifted by one oxygen. However, FI at *m/z* 90.0913 and at *m/z* 86.0964 representing the *N,N*-diethylmethylamine with and without the hydroxy-group emerged in the spectrum of metabolite B10. In comparison to the spectrum of the *N*-oxide (B9), those fragments were merely present in trace amounts. Nonetheless, we hypothesize that B10 consisted of an additional hydroxy group located at the indole core along with a *N*-oxide based on the comparably late Rt. The second phase II metabolite of 4-AcO-DET was generated by *O*-deacetylation, glucuronidation plus additional hydroxylation (B12, PI at *m/z* 425.1918). The MS^2 spectrum contained only two distinctive FI at *m/z* 176.0706 together with FI at *m/z* 86.0964 similar to the hydroxy metabolites indicating a hydroxylation at the indole core.

By comparing both *in vitro* and *in vivo* metabolism models, seven metabolites of 1cP-LSD were identified in pHLS9 whereas only three metabolites in ZL (see Table 1). The opposite case held true for 4-AcO-DET, the number of detected *in vivo* metabolites clearly exceeded the number of those detected *in vitro* (12 versus 5, see Table 2). The pHLS9 model produced only unique metabolic biomarkers of 1cP-LSD as all *in vitro* 4-AcO-DET metabolites included an *O*-deacetylation, which could also be produced by related compounds. However, in the ZL model, compound specific metabolites were identified for both NPS, which may serve as biomarkers after suspected consumption. For that purpose, 1cP-LSD metabolites, *N*-deethyl- (A5) and *N*-demethyl 1cP-LSD (A6), both found in *in vitro* and *in vivo* models, together with the parent compound, may be suitable targets. Notably, an adequate sample preparation and sensitive MS method is required to ensure the detection of 1cP-LSD and its metabolites in human material based on a detectability study in rat urine of other LSD-type NPS [25]. In terms of 4-AcO-DET, metabolites formed by *N*-deethylation (B2), hydroxylation (B7, B8), and *N*-oxidation (B9), seemed most appropriate as 4-AcO-DET markers.

Table 1
List of 1cP-LSD metabolites detected in pooled human liver S9 fraction (pHLS9) incubations after 1 and 6 h and in zebrafish larvae (ZL) after microinjection and 1 h-incubation. Data are represented as mean of absolute peak areas ($n = 2$) recorded in full-scan mode. The three largest areas per model and time are given in bold. Metabolite ID according to Table S1. n. d., not detected.

Metabolite ID	pHLS9 incubation [25 μM]		ZL microinjection [5 mM]
	1 h	6 h	
1cP-LSD	**2.2E+09**	**2.5E+08**	**5.6E+08**
A1 (*N*-deacyl-*N*-deethyl-)	2.2E+05	1.3E+06	n. d.
A2 (*N*-deacyl-*N*-demethyl-)	n. d.	1.7E+05	n. d.
A3 (*N*-deacyl-)	**9.7E+08**	**1.1E+09**	**7.4E+06**
A4 (*N*-deacyl-hydroxy-)	**1.3E+07**	**3.3E+07**	n. d.
A5 (*N*-deethyl-)	7.8E+06	3.8E+06	**4.0E+05**
A6 (*N*-demethyl-)	2.0E+06	5.9E+06	3.6E+05
A7 (hydroxy-)	2.8E+05	6.6E+05	n. d.

Table 2
List of 4-AcO-DET metabolites detected in pHLS9 incubations after 1 and 6 h and in zebrafish larvae (ZL) after exposure via immersion bath followed by 24 h-incubation. Data are represented as mean of absolute peak areas (n = 2) recorded in full-scan mode. The three largest areas per model and time are given in bold. Metabolite ID according to Table S2. n. d., not detected.

Metabolite ID	pHLS9 incubation [25 μM]		ZL immersion bath [100 μM]
	1 h	6 h	
4-AcO-DET	**1.3E+09**	**8.9E+08**	**9.4E+09**
B1 (*O*-deacetyl-)	**5.9E+09**	**6.4E+09**	**5.2E+09**
B2 (*N*-deethyl-)	n. d.	n. d.	1.3E+08
B3 (*O*-deacetyl-hydroxy isomer 1)	2.3E+07	**6.6E+07**	2.2E+08
B4 (*O*-deacetyl-hydroxy isomer 2)	n. d.	n. d.	4.3E+07
B5 (*O*-deacetyl-hydroxy isomer 3)	**7.3E+07**	3.2E+07	2.4E+07
B6 (*O*-deacetyl-*N*-oxide)	2.0E+07	2.7E+07	8.5E+07
B7 (hydroxy- isomer 1)	n. d.	n. d.	8.6E+06
B8 (hydroxy- isomer 2)	n. d.	n. d.	1.3E+07
B9 (*N*-oxide)	n. d.	n. d.	2.4E+08
B10 (hydroxy-*N*-oxide)	n. d.	n. d.	3.1E+06
B11 (*O*-deacetyl-glucuronide)	6.8E+06	2.1E+07	**4.3E+08**
B12 (*O*-deacetyl-hydroxy-glucuronide)	n. d.	n. d.	3.1E+06

3.4. Contribution of monooxygenases on initial metabolic steps

Ten CYP isozymes, most relevant on the xenobiotic metabolism, and FMO3 were used to assess their contribution on the initial metabolic reactions of the two hallucinogenic NPS. As represented in Table 3, all three initial metabolic reactions of 1cP-LSD were catalyzed by CYP2C8, 3A4, and 3A5, namely *N*-deethyl 1cP-LSD (A5), *N*-demethyl 1cP-LSD (A6), and hydroxy 1cP-LSD (A7). The isoform CYP1A2 was additionally involved in the formation of the *N*-deethyl- and *N*-demethyl-metabolites. Moreover, CYP2C19 also catalyzed the *N*-deethylation of 1cP-LSD. *N*-Deacylation was found to be a CYP-independent reaction as already observed for other LSD derivatives [25]. The low number of isoenzymes involved in the initial metabolic steps of 1cP-LSD might have a relevance for intoxication cases, particularly since inhibition of CYP1A2 and 3A4 resulted in a significant reduction of CYP-dependent metabolism of the structural related 1P-LSD [25].

The formation of *N*-deethyl 4-AcO-DET (B2) was catalyzed by CYP1A2, 2C8, 2C19, 2D6, and 3A4 as depicted in Table 4. Both hydroxy isomers (B7 and B8) were formed by CYP1A2 and CYP3A4 and additionally B7 by CYP2B6, 2D6, and 2A6, and B8 by 3A5. CYP2C9, 3A4, and FMO3 were involved on the *N*-oxide formation (B9). In general, several isoforms contributed to initial metabolic steps of 4-AcO-DET, hence the risk of intoxications either by co-consumption with other drugs (of abuse) or by interindividual differences should be rather low.

3.5. Hepatotoxic potential using HepG2 cells

A HCSA method was used measuring six different biomarkers with four fluorescent dyes to assess the *in vitro* hepatotoxic potential of the psychedelic NPS. Hoechst33342, a DNA-binding dye, was used to stain the cell nuclei for monitoring of the cell number, morphological changes in the nuclei, and the nuclear intensity. The mitochondrial membrane potential was measured using the positively charged TMRM dye, which loads into the negatively charged mitochondria. Therefore, a disturbed mitochondrial membrane potential correlates with a reduced or heightened TMRM intensity. As a note, the used positive control, FCCP, leads to a reduced TMRM signal. The calcium sensitive dye, CAL-520 AM, specifically binds to intracellular calcium as a protective ester group prevents unselective binding to extracellular calcium. Once passed through the cell membrane CAL-520 AM is cleaved by esterases in the cytoplasm. An enhanced fluorescent signal of CAL-520 indicates

Table 3
Contribution of cytochrome P450 (CYP) monooxygenases and flavin-containing monooxygenase (FMO) 3 on the initial metabolic reactions of 1cP-LSD. Metabolite ID according to Table S1. +, detected, -, not detected.

Metabolite ID	CYP										FMO
	1A2	2A6	2B6	2C8	2C9	2C19	2D6	2E1	3A4	3A5	3
A5 (*N*-deethyl-)	+	-	-	+	-	+	-	-	+	+	-
A6 (*N*-demethyl-)	+	-	-	+	-	-	-	-	+	+	-
A7 (hydroxy-)	-	-	-	+	-	-	-	-	+	+	-

Table 4
Contribution of cytochrome P450 (CYP) monooxygenases and flavin-containing monooxygenase (FMO) 3 on the initial metabolic reactions of 4-AcO-DET. Metabolite ID according to Table S2. +, detected; -, not detected.

Metabolite ID	CYP										FMO
	1A2	2A6	2B6	2C8	2C9	2C19	2D6	2E1	3A4	3A5	3
B2 (*N*-deethyl-)	+	-	-	+	-	+	+	-	+	-	-
B7 (hydroxy- isomer 1)	+	-	+	-	-	-	+	-	+	-	-
B8 (hydroxy- isomer 2)	+	+	-	-	-	-	-	-	+	+	-
B9 (*N*-oxide)	-	-	-	-	+	-	-	-	+	-	+

binding of Ca^{2+} released from intracellular storages or entering the cell from the extracellular bath solution through an impaired plasma membrane. The second nucleic acid stain, TOTO-3, is cell-impermeable for viable cells. When cells are damaged, TOTO-3 binds to both single- and double-stranded DNA. A higher intensity of TOTO-3 therefore corresponds to an increased rate of dead cells.

Fig. 3 contains the dose-response plots of the six parameters obtained after incubation of 1cP-LSD (A) and 4-AcO-DET (B) with HepG2 cells for 48 h at a low (3.15 or 7.81 μM) and high (50 or 125 μM) concentration. In this section, only the white bars without ABT will be discussed. No cytotoxic parameters were significantly affected by 1cP-LSD, except for the mitochondrial membrane potential which was increased at the low 1cP-LSD concentration. Even though some concentration-dependent effects on parameters were observed, e.g., by a slight increase of the intracellular calcium levels or decrease of the nuclear intensity, lower concentrations are expected in human plasma for LSD-related compounds [28]. Apart from that, the intake of standard LSD doses has been considered as safe and "non-toxic" for consumers [31]. However, little is known about the pharmacology and toxicology of 1cP-LSD. A HTR study in mice reported about an LSD-like behavior *in vivo* with a comparable potency to 1 P-LSD but reduced potency by 69 % compared with LSD [3].

Basically, the outcome of the hepatoxicity study for 4-AcO-DET was like 1cP-LSD. The tryptamine-related compound caused no significant alterations on any parameters indicating no *in vitro* hepatotoxicity for 4-AcO-DET. So far, only one toxicity study exists reporting about an induced proliferation rate of 4-AcO-DET on cardiac cells in a concentration-dependent manner and increased QT intervals in rats amongst others [32]. In this regard, further toxicity studies with focus on other organ systems are requested to forecast potential harmful effects of NPS.

3.6. Metabolism-based effects on the hepatotoxicity

The unspecific CYP-inhibitor ABT has been previously used to study CYP-based effects on HepG2 cells by biotransformation products of xenobiotics [21,23]. Due to the lack of data, the applied ABT concentration was based on studies using other cell lines than HepG2 without even knowing whether this concentration is sufficient to inhibit CYP enzymes in HepG2 cells. That leads to the basic question whether HepG2 cells are able to produce considerable amounts of metabolites based on its rather low gene expression levels of CYP enzymes compared with other human hepatic cell types [33]. To clear things up, the CYP enzyme activity in HepG2 cells in the absence and presence of ABT in different concentrations (0 − 1000 μM) were determined using an adapted CYP substrate cocktail assay [24]. The following CYP enzymes were tested: CYP1A2 (phenacetine), 2B6 (bupropion), 2C9 (diclofenac), 2C19 (omeprazole), 2D6 (dextromethorphan), 3 A (testosterone) [24]. As depicted in Fig. S3 in the ESM, the enzyme activity was plotted as peak area ratio of the respective metabolite of the specific CYP substrate to the IS normalized to the total protein amount. Only CYP2C19, 2D6, and 3 A showed a notable activity in our assay. Inhibitory effects of ABT on the enzyme activities were already visible at the lowest test concentration at 10 μM which increased in a concentration-dependent manner. To ensure that the finally selected ABT concentration shows no harmful effects on HepG2 cells, in a second step, cytotoxic effects of ABT (0 − 1000 μM) were tested using the same HCSA approach as applied for the NPS. No significant changes in parameters were obtained for ABT concentrations below 500 μM (Fig. S4 in the ESM). At 1000 μM the nuclear size and mitochondrial membrane potential were significantly reduced. Furthermore, the cell count was reduced at concentrations of 500 and 1000 μM but without statistical significance. However, high variations in the cell count have been also observed in previous studies which might result from inconsistencies during cell seeding, e.g., insufficient mixing of the cell suspension [23]. Finally, an ABT concentration of 500 μM was selected to study metabolism-based effects on the cytotoxicity of NPS. Since this concentration is expected to effectively inhibit CYP enzymes and to induce no toxic signs on HepG2 cells.

In this section, the grey bars (without ABT) represented in Fig. 3 will be compared to the white bars (with ABT) containing the same NPS concentration. For 1cP-LSD (A), no significant results were obtained suggesting that neither the parent compound nor its metabolites possess an *in vitro* cytotoxic potential. In case of 4-AcO-DET (B), two parameters, nuclear size and cytosolic calcium levels, were significantly increased in incubations containing a high 4-AcO-DET concentration (125 μM) with ABT compared with incubations containing 125 μM 4-AcO-DET without ABT. Having said that, the rise in CAL-520 intensity was less pronounced for 4-AcO-DET than for the positive control FCCP. Since knowledge about intracellular concentrations of NPS is fundamentally important to toxicity, but are hardly available in human, typically blood or plasma concentrations are used as surrogate measure [34]. Plasma concentrations of 4-AcO-DET were not available, thus test concentrations were compared to plasma concentrations of related tryptamine analogues (0.4−0.9 μM) [35–37]. These were below the test concentrations, making relevant metabolism-dependent cytotoxic events in human rather unlikely. However, intracellular compound concentrations do not necessarily equate to plasma concentrations as those depend on further toxicokinetic parameters, such as active transports [34].

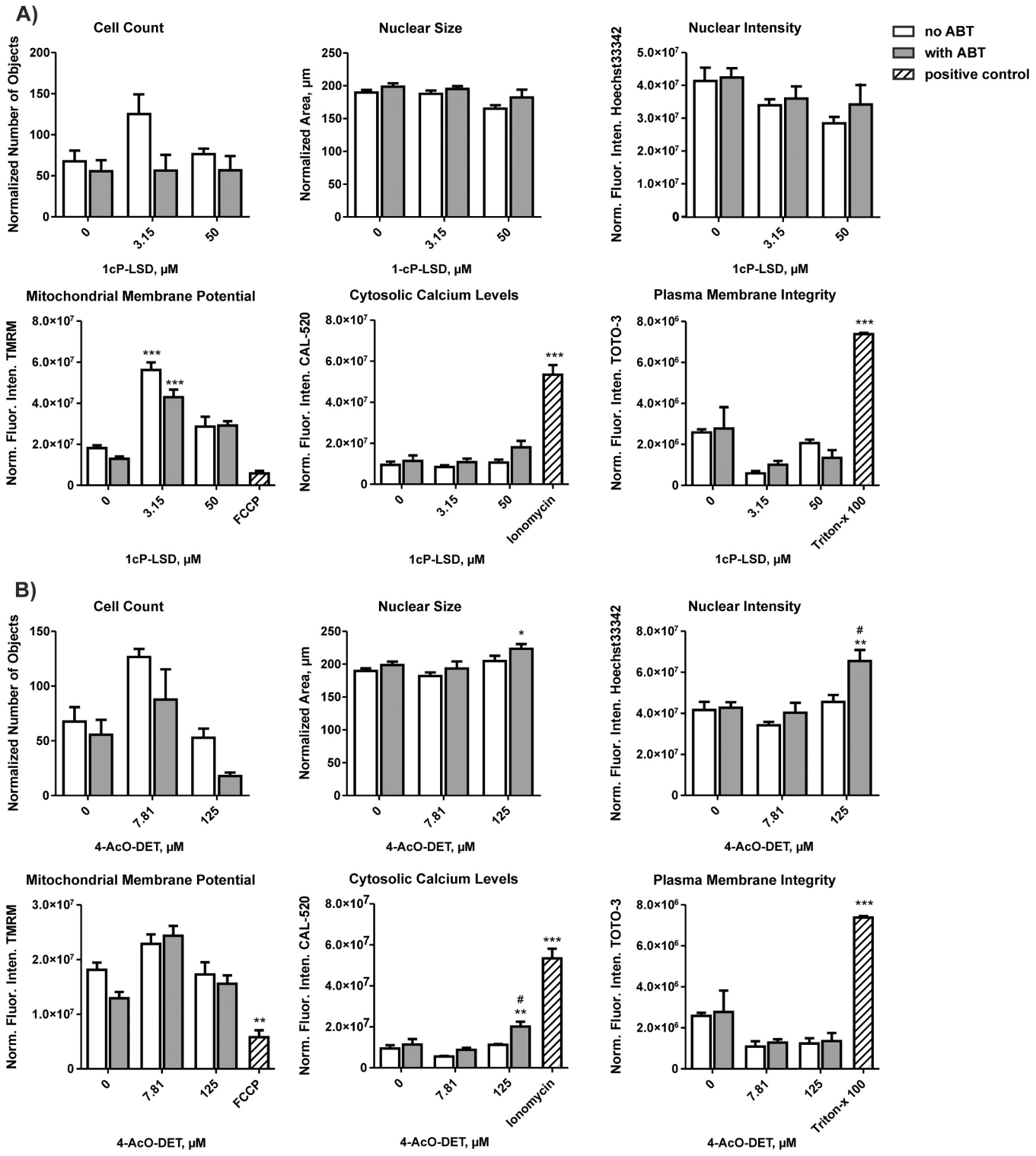

Fig. 3. Dose-response plots of 1cP-LSD (A) and 4-AcO-DET (B) obtained after incubation with HepG2 cells for 48 h at a low (3.15 or 7.81 µM) and high (50 or 125 µM) concentration and blank incubations without NPS both without (white bars) and with (grey bars) the cytochrome P450-inhibitor 1-aminobenzotriazol (ABT) and the positive controls FCCP, ionomycine, and Triton-X 100, respectively. Changes in different parameters (cell count, nuclear size, nuclear intensity, mitochondrial membrane potential, cytosolic calcium levels, and plasma membrane integrity) are plotted as absolute values. All parameters were normalized to the cell count except the cell count, which was normalized to the number of appropriate images. Values are expressed as mean ± standard error of the mean (SEM; $n = 5$). Statistical analysis was done using one-way ANOVA followed by Tuckey's post-hoc test (***, $P < 0.001$, **, $P < 0.01$, *, $P < 0.05$ blank incubations without NPS and ABT versus all other incubations; $^{\#}$, $P < 0.05$ NPS incubations versus *NPS* incubations plus ABT at the same concentration). Norm. Fluor. Inten., normalized fluorescence intensity.

4. Conclusion

The present study demonstrated that 1cP-LSD and 4-AcO-DET were metabolized to several phase I and in case of 4-AcO-DET to additional phase II metabolites in both the pHLS9 and ZL model. The ZL model, after microinjection, provided less 1cP-LSD metabolites than pHLS9, whereas most metabolites of 4-AcO-DET were identified in ZL after immersion bath exposure compared to pHLS9. Several metabolites of both hallucinogens can be formed from many other NPS but specific metabolites have also been identified in this study that overcome this problem. No direct cytotoxic effects of 1cP-LSD and 4-AcO-DET could be observed in HepG2 cells at concentrations above expected consumer dosages, but metabolism-dependent effects of 4-AcO-DET were indicated and cannot be excluded.

CRediT authorship contribution statement

Sari Rasheed: Conceptualization, Methodology, Supervision, Writing – review & editing. **Lea Wagmann:** Methodology, Writing – review & editing. **Jonas Baumann:** Methodology, Writing – review & editing. **Folker Westphal:** Resources, Writing – review & editing. **Benedikt Pulver:** Resources, Writing – review & editing. **Rolf Müller:** Resources, Writing – review & editing. **Veit Flockerzi:** Resources, Writing – review & editing. **Tanja M Gampfer:** Conceptualization, Methodology, Project administration, Writing – original draft. **Markus R. Meyer:** Conceptualization, Methodology, Resources, Supervision, Writing – review & editing. **Philip Schippers:** Investigation, Methodology, Supervision, Writing – review & editing. **Victoria Schütz:** Formal analysis, Investigation.

Declaration of Competing Interest

The authors declare the following financial interests/personal relationships which may be considered as potential competing interests: Veit Flockerzi reports financial support was provided by German Research Foundation. If there are other authors, they declare that they have no known competing financial interests or personal relationships that could have appeared to influence the work reported in this paper.

Acknowledgements

The authors would like to thank Simon D. Brandt, Yu Mi Park, Anna-Lena Gehl, Claudia Fecher-Trost, Carsten Schröder, Gabriele Ulrich, Marnie F. Cole, and Heidi Löhr for their support, the EU funded Project ADEBAR plus (grant no.: IZ25–5793-2019-33) for the supply of chemical standard and Fabian Frankenfeld for proofreading. We acknowledge support by the Deutsche Forschungsgemeinschaft (DFG, German Research Foundation) SFB 894 (project ID 157660137, A14 to V.F.).

Appendix A. Supporting information

Supplementary data associated with this article can be found in the online version at doi:10.1016/j.jpba.2024.116187.

References

[1] A.Y. Simão, M. Antunes, E. Cabral, P. Oliveira, L.M. Rosendo, A.T. Brinca, E. Alves, H. Marques, T. Rosado, L.A. Passarinha, M. Andraus, M. Barroso, E. Gallardo, An update on the implications of new psychoactive substances in public health, Int. J. Environ. Res. Public Health 19 (2022).

[2] EMCDDA. European Drug Report 2023. Publications of of the European Union, Luxembourg, 2023. https://www.emcdda.europa.eu/publications/european-drug-report/2023_en. Accessed April 2024.

[3] S.D. Brandt, P.V. Kavanagh, F. Westphal, A. Stratford, A.U. Odland, A.K. Klein, G. Dowling, N.M. Dempster, J. Wallach, T. Passie, A.L. Halberstadt, Return of the lysergamides. Part VI: analytical and behavioural characterization of 1-cyclopropanoyl-d-lysergic acid diethylamide (1CP-LSD), Drug Test. Anal. 12 (2020) 812–826.

[4] L.B. Kozell, A.J. Eshleman, T.L. Swanson, S.H. Bloom, K.M. Wolfrum, J. L. Schmachtenberg, R.J. Olson, A. Janowsky, A.I. Abbas, Pharmacologic activity of substituted tryptamines at 5-hydroxytryptamine (5-HT)(2A) Receptor (5-HT(2A) R), 5-HT(2C)R, 5-HT(1A)R, and serotonin transporter, J. Pharmacol. Exp. Ther. 385 (2023) 62–75.

[5] N. Theofel, P. Möller, E. Vejmelka, C. Kramer, M. Tsokos, S. Scholtis, A fatal case report resulting from the abuse of the designer benzodiazepines clonazolam and flualprazolam in conjunction with dried opium poppy pods, J. Anal. Toxicol. 46 (2023) e285–e290.

[6] F.T. Peters, M.R. Meyer, In vitro approaches to studying the metabolism of new psychoactive compounds, Drug Test. Anal. 3 (2011) 483–495.

[7] T.M. Gampfer, L. Wagmann, M.J. Richter, S. Fischmann, F. Westphal, M.R. Meyer, Toxicokinetic studies and analytical toxicology of the new synthetic opioids cyclopentanoyl-fentanyl and tetrahydrofuranoyl-fentanyl, J. Anal. Toxicol. 44 (2020) 449–460.

[8] L.H.J. Richter, J. Herrmann, A. Andreas, Y.M. Park, L. Wagmann, V. Flockerzi, R. Muller, M.R. Meyer, Tools for studying the metabolism of new psychoactive substances for toxicological screening purposes - a comparative study using pooled human liver S9, HepaRG cells, and zebrafish larvae, Toxicol. Lett. 305 (2019) 73–80.

[9] Y.M. Park, M.R. Meyer, R. Muller, J. Herrmann, Drug administration routes impact the metabolism of a synthetic cannabinoid in the zebrafish larvae model, Molecules 25 (2020).

[10] L. Wagmann, T.M. Gampfer, M.R. Meyer, Recent trends in drugs of abuse metabolism studies for mass spectrometry-based analytical screening procedures, Anal. Bioanal. Chem. 413 (2021) 5551–5559.

[11] S. Cassar, I. Adatto, J.L. Freeman, J.T. Gamse, I. Iturria, C. Lawrence, A. Muriana, R.T. Peterson, S. Van Cruchten, L.I. Zon, Use of zebrafish in drug discovery toxicology, Chem. Res. Toxicol. 33 (2020) 95–118.

[12] S. Rasheed, F. Fries, R. Müller, J. Herrmann, Zebrafish: An attractive model to study Staphylococcus aureus infection and its use as a drug discovery tool, Pharmaceuticals(Basel) 14 (2021).

[13] F. Sewell, J. Edwards, H. Prior, S. Robinson, Opportunities to apply the 3Rs in safety assessment programs, Ilar J. 57 (2016) 234–245.

[14] D. Martins, E. Gil-Martins, F. Cagide, C. da Fonseca, S. Benfeito, C. Fernandes, D. Chavarria, F. Remião, R. Silva, F. Borges, Unraveling the in vitro toxicity profile of psychedelic 2C phenethylamines and their N-benzylphenethylamine (NBOMe) analogues, Pharmaceuticals (Basel) 16 (2023).

[15] V. Sogos, P. Caria, C. Porcedda, R. Mostallino, F. Piras, C. Miliano, M.A. De Luca, M.P. Castelli, Human neuronal cell lines as an in vitro toxicological tool for the evaluation of novel psychoactive substances, Int. J. Mol. Sci. 22 (2021).

[16] P.J. O'Brien, A. Edvardsson, Validation of a multiparametric, high-content-screening assay for predictive/investigative cytotoxicity: evidence from technology transfer studies and literature review, Chem. Res. Toxicol. 30 (2017) 804–829.

[17] L.H.J. Richter, A. Beck, V. Flockerzi, H.H. Maurer, M.R. Meyer, Cytotoxicity of new psychoactive substances and other drugs of abuse studied in human HepG2 cells using an adopted high content screening assay, Toxicol. Lett. 301 (2019) 79–89.

[18] L. Wagmann, F. Frankenfeld, Y.M. Park, J. Herrmann, S. Fischmann, F. Westphal, R. Muller, V. Flockerzi, M.R. Meyer, How to study the metabolism of new psychoactive substances for the purpose of toxicological screenings-a follow-up study comparing pooled human liver S9, HepaRG cells, and zebrafish larvae, Front Chem. 8 (2020) 539.

[19] U. Strähle, S. Scholz, R. Geisler, P. Greiner, H. Hollert, S. Rastegar, A. Schumacher, I. Selderslaghs, C. Weiss, H. Witters, T. Braunbeck, Zebrafish embryos as an alternative to animal experiments–a commentary on the definition of the onset of protected life stages in animal welfare regulations, Reprod. Toxicol. 33 (2012) 128–132.

[20] T.M. Gampfer, L. Wagmann, Y.M. Park, A. Cannaert, J. Herrmann, S. Fischmann, F. Westphal, R. Muller, C.P. Stove, M.R. Meyer, Toxicokinetics and toxicodynamics of the fentanyl homologs cyclopropanoyl-1-benzyl-4 -fluoro-4-anilinopiperidine and furanoyl-1-benzyl-4-anilinopiperidine, Arch. Toxicol. 94 (2020) 2009–2025.

[21] T.M. Gampfer, L. Wagmann, A. Belkacemi, V. Flockerzi, M.R. Meyer, Cytotoxicity, metabolism, and isozyme mapping of the synthetic cannabinoids JWH-200, A-796260, and 5F-EMB-PINACA studied by means of in vitro systems, Arch. Toxicol. 95 (2021) 3539–3557.

[22] M.J. Richter, L. Wagmann, T.M. Gampfer, S.D. Brandt, M.R. Meyer, In vitro metabolic fate of the synthetic cannabinoid receptor agonists QMPSB and QMPCB (SGT-11) including isozyme mapping and esterase activity, Metabolites 11 (2021).

[23] T.M. Gampfer, L. Wagmann, B. Pulver, F. Westphal, V. Flockerzi, M.R. Meyer, A simplified strategy to assess the cytotoxicity of new psychoactive substances in HepG2 cells using a high content screening assay - Exemplified for nine compounds, Toxicology 476 (2022) 153258.

[24] J. Dinger, M.R. Meyer, H.H. Maurer, Development of an in vitro cytochrome P450 cocktail inhibition assay for assessing the inhibition risk of drugs of abuse, Toxicol. Lett. 230 (2014) 28–35.

[25] L. Wagmann, L.H.J. Richter, T. Kehl, F. Wack, M.P. Bergstrand, S.D. Brandt, A. Stratford, H.H. Maurer, M.R. Meyer, In vitro metabolic fate of nine LSD-based new psychoactive substances and their analytical detectability in different urinary screening procedures, Anal. Bioanal. Chem. 411 (2019) 4751–4763.

[26] L. Perrin, N. Loiseau, F. André, M. Delaforge, Metabolism of N-methyl-amide by cytochrome P450s: formation and characterization of highly stable carbinol-amide intermediate, Febs J. 278 (2011) 2167–2178.

[27] R. Martin, J. Schürenkamp, H. Pfeiffer, H. Köhler, A validated method for quantitation of psilocin in plasma by LC-MS/MS and study of stability, Int. J. Leg. Med. 126 (2012) 845–849.

[28] P.C. Dolder, Y. Schmid, A.E. Steuer, T. Kraemer, K.M. Rentsch, F. Hammann, M. E. Liechti, Pharmacokinetics and pharmacodynamics of lysergic acid diethylamide in healthy subjects, Clin. Pharmacokinet. 56 (2017) 1219–1230.
[29] C. de Souza Anselmo, V.F. Sardela, V.P. de Sousa, H.M.G. Pereira, Zebrafish (Danio rerio): a valuable tool for predicting the metabolism of xenobiotics in humans? Comp. Biochem. Physiol. C. Toxicol. Pharmacol. 212 (2018) 34–46.
[30] E. Küster, Cholin- and carboxylesterase activities in developing zebrafish embryos (Danio rerio) and their potential use for insecticide hazard assessment, Aquat. Toxicol. 75 (2005) 76–85.
[31] D.E. Nichols, C.S. Grob, Is LSD toxic? Forensic Sci. Int. 284 (2018) 141–145.
[32] K.S. Yoon, J.M. Lee, Y.H. Kim, S.K. Suh, H.J. Cha, Cardiotoxic effects of [3-[2-(diethylamino)ethyl]-1H-indol-4-yl] acetate and 3-[2-[ethyl(methyl)amino]ethyl]-1H-indol-4-ol, Toxicol. Lett. 319 (2020) 40–48.
[33] S.N. Hart, Y. Li, K. Nakamoto, E.A. Subileau, D. Steen, X.B. Zhong, A comparison of whole genome gene expression profiles of HepaRG cells and HepG2 cells to primary human hepatocytes and human liver tissues, Drug Metab. Dispos. 38 (2010) 988–994.
[34] X. Chu, K. Korzekwa, R. Elsby, K. Fenner, A. Galetin, Y. Lai, P. Matsson, A. Moss, S. Nagar, G.R. Rosania, J.P. Bai, J.W. Polli, Y. Sugiyama, K.L. Brouwer, Intracellular drug concentrations and transporters: measurement, modeling, and implications for the liver, Clin. Pharmacol. Ther. 94 (2013) 126–141.
[35] L. Wagmann, S.K. Manier, M.R. Meyer, Can the intake of a synthetic tryptamine be detected only by blood plasma analysis? A clinical toxicology case involving 4-HO-MET, J. Anal. Toxicol. (2021).
[36] K.E. Grafinger, M. Hadener, S. Konig, W. Weinmann, Study of the in vitro and in vivo metabolism of the tryptamine 5-MeO-MiPT using human liver microsomes and real case samples, Drug Test. Anal. (2017).
[37] M. Good, Z. Joel, T. Benway, C. Routledge, C. Timmermann, D. Erritzoe, R. Weaver, G. Allen, C. Hughes, H. Topping, A. Bowman, E. James, Pharmacokinetics of N,N-dimethyltryptamine in Humans, Eur. J. Drug Metab. Pharmacokinet. 48 (2023) 311–327.